Available online at website: https://journal.bcrec.id/index.php/bcrec

Bulletin of Chemical Reaction Engineering & Catalysis, 21 (1) 2026, 213-225

Original Research Article

Crystal Phase-Dependence of Ru@TiO_2 Catalysts on the Product Selectivity in the Aqueous Phase Hydrogenolysis of Furfuryl Alcohol

Thea Seventina Desiani Bodoi[1], Shauqi Aulia Rifwanda[1], Rodiansono Rodiansono[1,2*], Atina Sabila Azzahra[2,3], Utami Irawati[1], Ferensa Oemry[4], Gagus Ketut Sunnardianto[4], Indri Badria Adilina[5,6], Takayoshi Hara[7*]

[1]Department of Chemistry, Lambung Mangkurat University, Jl. A. Yani Km 36,0 Banjarbaru 70714, Banjarbaru, Indonesia.
[2]Catalysis for Sustainable Energy and Environment (CATSuRe), Inorganic Materials and Catalysis (IMCat) Laboratory, Lambung Mangkurat University, Jl. A. Yani Km 36,0 Banjarbaru 70714, Indonesia.
[3]School of Chemistry, Joseph Black Building. University of Glasgow, Glasgow, G12 SQQ, United Kingdom.
[4]Research Centre for Quantum Physics, BRIN, KST BJ Habibie, Serpong, Tangerang Selatan, Indonesia.
[5]Research Centre for Chemistry, BRIN, KST BJ Habibie, Serpong, Tangerang, Indonesia.
[6]Research Centre for Catalysis, BRIN, KST BJ Habibie, Serpong, Tangerang, Indonesia.
[7]Department of Applied Chemistry and Biotechnology, Graduate School of Engineering, Chiba University, 1-33, Yayoi-cho, Inage-ku, Chiba 263-8522, Japan.

Received: 28th November 2025; Revised: 14th January 2026; Accepted: 15th January 2026
Available online: 17th January 2026; Published regularly: April 2026

Abstract

The crystal phase-dependence of ruthenium supported on titania (Ru@TiO_2) catalysts on the product selectivity in the aqueous phase hydrogenolysis of furfuryl alcohol (FFalc) was investigated. The supported ruthenium nanoparticles (RuNPs) catalysts on TiO_2 with different phases, *c.a.* rutile (R), anatase (A), and brookite (B) were employed. The Ru@TiO_2(R) catalysed the hydrogenation-rearrangement reaction of furan ring to afford cyclopentanone/cyclopentanol (CPO/CPL) as the main product. The presence of high surface acidity in Ru@TiO_2(R) catalyst promoted the hydrogenation-rearrangement of furan ring leading to CPO/CPL as the main product as indicated by NH_3-TPD and pyridine-ATR-IR results. In contrast, the Ru@TiO_2(A) catalyst selectively hydrogenolysed the furan ring to produce 1,5-pentanediol (1,5-PeD). This high selectivity of 1,5-PeD over Ru@TiO_2(A) catalyst may be affected by the high dispersion of Ru NPs on TiO_2 facets as depicted by the high H_2-uptake and small particle sizes.

Keywords: TiO_2 facets; furfuryl alcohol; hydrogenolysis-rearrangement; CPO/CPL, 1,5-pentanediol

How to Cite: Bodoi, T. S. D., Rifwanda, S. A., Rodiansono, R., Azzahra, A. S., Irawati, U., Oemry, F., Sunnardianto, G. K., Adilina, I. B., Hara, T. (2026). Crystal Phase-Dependence of Ru@TiO_2 Catalysts on the Product Selectivity in the Aqueous Phase Hydrogenolysis of Furfuryl Alcohol. *Bulletin of Chemical Reaction Engineering & Catalysis*, 21 (1), 213-225. (DOI: 10.9767/bcrec.20547)

Permalink/DOI: https://doi.org/10.9767/bcrec.20547

1. Introduction

The development of selective heterogeneous catalysts for the efficient transformation of biomass-derived platform furfural (FFald) into α,ω-diols such as 1,2-, 1,4- or 1,5-pentanediol (PeD) has been attracted great attentions [1,2]. Since the furan ring consisted of two reactive functional groups; terminal aldehyde (C=O) and unsaturated furang ring (C=C), the reaction of FFald involved two-competitive reaction steps: (1) hydrogenation of C=O and C=C bonds to THFalc or (2) direct furan ring cleavage to 1,2-PeD and 1,5-PeD, which the major product of diols was depended on the catalyst properties and reaction conditions (**Scheme 1**) [3–5]. However, achieving

* Corresponding Author.
Email: rodiansono@ulm.ac.id (R. Rodiansono);
t_hara@faculty.chiba-u.jp (Takayoshi Hara)

a high selectivity and high yield synthesis of 1,2-PeD or 1,5-PeD from either FFald or FFalc is challenging due to the reactivity of the furan ring and the complex interactions on the catalyst surface [6–8]. Tomishige *et al.* highlighted that increasing the selectivity of 1,5-PeD or 1,2-PeD from FFalc is associated with metal active sites and the basicity or acidity of catalysts used [5]. Nevertheless, metal-acid catalysts with strong acidity led to the hydrogenative rearrangement of furan ring to C5-cyclic compounds such as cyclopentanone (CPO) or cyclopentanol (CPL) [9]. Consequently, designing and controlling the selectivity of catalyst towards hydrogenative rearrangement to CPO/CPL or hydrogenolysis of furan ring to 1,2- or 1,5-PeD still remains a significant challenge.

Metal oxides, such as CeO_2, ZrO_2, or TiO_2 supported-PGM catalysts, played important role in the selective hydrogenation/hydrogenolysis FFald, FFalc, or THFalc to 1,2-PeD or 1,5-PeD [10–12]. For instance, Pt/CeO_2-nanocubes with the ceria-terminal facets exposed (100) afforded higher 1,2-PeD yield (77%) than that of Pt/CeO-nanorods and Pt/CeO-octahedron catalysts [11,12]. The dispersion of Ru nanoparticles (RuNPS) on rutile(r)-TiO_2 appeared to be higher dispersion and narrow sizes distribution due to strong interaction between RuO_2 and r-TiO_2 during thermal treatment. As the results, Ru/r-TiO_2 exhibited higher activity and thermal stability than that of Ru/anatase(a)-TiO_2 catalyst in CO_2 methanation [13]. Similarly, Mageed *et al.* reported that the selectivity product of CO_2 methanation over Ru/r-TiO_2 catalysts are driven by the temperature reduction, Ru metal loading amount as well as the dispersion on TiO_2. Therefore, controlling the catalytic properties by varying the support particle size, is of general relevance for a larger number of catalysts and reactions [14]. Furthermore, crystal-phase-depended strong metal-interaction of TiO_2 supported-metal catalysts enhanced hydrodeoxygenation of m-cresol as a function of temperature reduction during the catalyst preparation as reported by Cui *et al.* [15]. Most recently Tan *et al.* reported that the aqueous phase hydrogenative-rearrangement of FFalc to CPO was crucially dictated by the Ni-O-Ti interface structure, governing nickel speciation and reactivity. Obviously, Ni on mixed-phase P25 exhibited highest FFalc conversion (91%) affording 89% CPO with specific rate of 72 h^{-1}, which much higher than that of Ni on pure anatase catalyst [16]. Most recently, Amin et al. highlighted that the selectivity of Ru/TiO_2 catalysts on the 5-hydroxymethylfurfural (HMF) reaction was strongly depended on morfological of TiO_2, dispersion of active metal (RuNPs), and exposure of active metal on surface of TiO_2. Catalyst of Ru/TiO_2 with larger surface area resulted higher dispersion of RuNPs and exhibited the hydrogenolysis of hydroxyl group to 5-methylfurfural (5-MF). On the other hand, Ru/TiO_2 catalyst with lower surface area and high particle sizes of RuNPs hydrogenated C=O as well as C=C bonds to produce 2,5-bis(hydroxylmethyl)furan (BHMF) and 2,5-bis(hydroxylmethyl)tetrahydofuran (BHMTHF) [17]. Therefore, controlling the dispersion and metal exposore on oxide supports is crucial for switching the activity and selectivity of furan reaction.

In the present report, the extended investigation on the effect of TiO_2 phase as the support of RuNPs catalysts for hydrogenolysis or hydrogenation-rearrangement of FFalc to the target product of diols (1,2-, 1,4-, or 1,5-PeD) or CPO/CPL. Motivated by the recent reports in our group, the modification of g-Al_2O_3 with TiO_2(A)

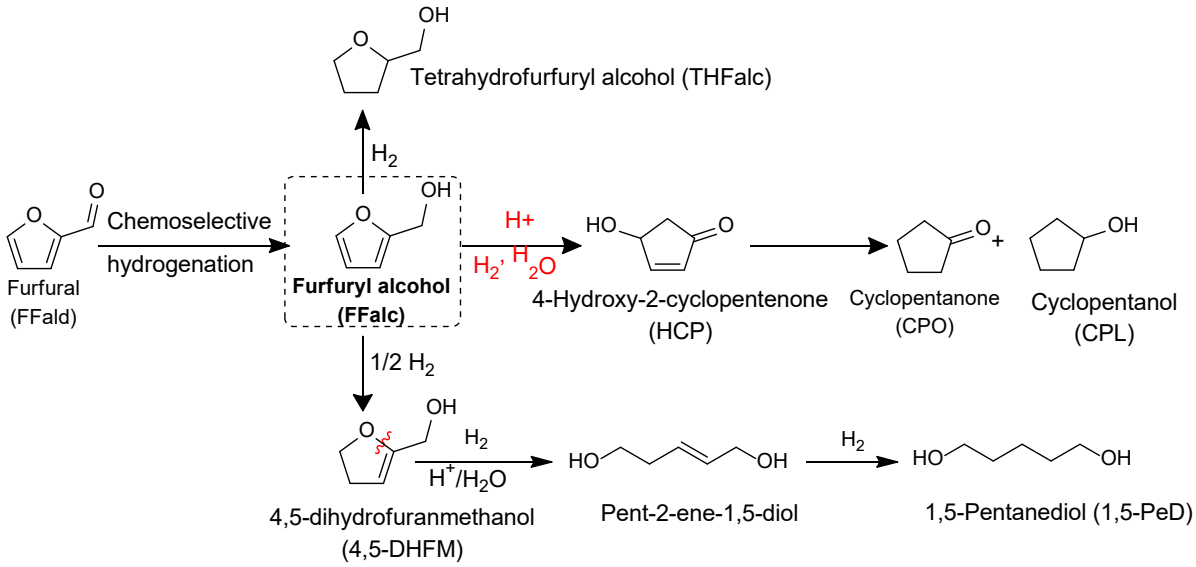

Scheme 1. Possible reaction pathways for the transformation of FFalc into high-added-value chemicals (e.g., CPO/CPL and 1,5-PeD) using heterogeneous Ru-based catalysts [18].

and TiO_2(R) as the support of Ru-Sn catalysts demonstrated a higher yield of 1,5-PeD with CPO/CPL as the minor product, depending on the type of TiO_2; anatase(A) or rutile(R) [19,20]. Herein, the crystal-phase dependence of ruthenium supported on titania c.a. Ru@TiO_2(R) and Ru@TiO_2(A) catalysts on the product selectivity in the aqueous phase hydrogenolysis of of has been investigated. The Ru@TiO_2(R) catalyst allowed to produce CPO/CPL (up to 82% yield), while the Ru@TiO_2(A) afforded 1,5-PeD (up to 80% yield) as the main product at 180 °C, initial H2 10-30 bar for 3-5 h. A series characterisation techniques, such as XRD, H_2-TPR, NH_3-TPD, and pyridine-ATR-IR, were employed to gain the catalytic results and catalyst structure-activity relationship and discussed systematically.

2. Materials and Methods

2.1 Materials

Ruthenium (III) chloride x hydrate ($RuCl_3 \cdot xH_2O$), furfuryl alcohol (95% GC), dodecane (99%), 2-methoxyethanol, ZrO_2, Nb_2O_5, and ZnO were purchased from Sigma Aldrich Co. The active charcoal (AC) (S_{BET} = 600 $m^2.g^{-1}$) and γ–Al_2O_3 (S_{BET} = 129 $m^2.g^{-1}$) were purchased from Merck Millipore Co. Sodium hydroxide (NaOH pellet, 99,0%) and ethanol (C_2H_5OH, 96%) were purchased from Sigma-Millipore. TiO_2 anatase (TiO_2(A)) and TiO_2 rutile (TiO_2(R)) were purchased and used as received from Hongwunewmaterial (HWNANO) Ltd Co.

2.2. Methods

2.2.1. Catalyst Preparation

Preparation of Ru@TiO_2(A): Typical procedure for the synthesis of Ru@TiO_2(A) (Ru = 4 wt%) is described as follows [21,22]. A 0.0768 g (0.3702 mmol) of ruthenium(III) chloride x hydrate ($RuCl_3 \cdot xH_2O$) was dissolved in deionised water at room temperature under gentle stirring. A one-gram TiO_2(A) and $RuCl_3$ solution were mixed at the room temperature, then the temperature was raised to 50 °C and kept in stirring for 12 h. The pH was adjusted to 9-10 by addition dropwise of an aqueous solution NaOH (3.1 M). The mixture was transferred to the sealed-Teflon autoclave reactor for hydrothermal processes at 150 °C for 24 h. The obtaining black (grey) solid precipitate was washed with distilled water and acetone, and then dried *in vacuo* at room temperature for overnight. Prior to characterisation and catalytic reaction, the black solid of Ru@TiO_2(A) was reduced with hydrogen at 400 °C for 2 h.

For comparison, the TiO_2 (B) support was prepared using a simple hydrolysis of $TiCl_4$ solution with concentrate HCl at room temperature to obtain a clear solution of $TiCl_4$. Around 20% of $TiCl_4$ was mixture with NaOH 6 M then transferred into the sealed-Teflon autoclave reactor for hydrothermal processes at 150 °C for 24 h. The obtained white precipitate was washed with distilled water and acetone and then dried in vacuo for overnight. Prior to use as support, the obtained white solid TiO_2 brookite was dried at 110 °C for 12 h, then followed by calcination 300 °C under N_2 for 2 h [21,23,24].

2.2.2. Catalyst Characterisations

The X-ray diffraction (XRD) analysis was performed on a Miniflex 600 Rigaku instrument with Cu as monochromatic source of Cu-Kα radiation (λ = 0.1544 nm). The XRD was operated at 40 kV and 15 mA with a step width of 0.02°, a scan speed of 4° min^{-1} (a_1 = 0.1540 nm, a_2 = 0.1544 nm), solar slit 1.25°, and using a Ni Kβ filter. Inductively-coupled plasma atomic emission spectroscopy (ICP-AES) measurements were performed on an SPS 1800H plasma spectrometer by Seiko Instruments Inc. Japan (Ru: 267.87 nm and Ti: 337.280 nm) at Chiba University. Scanning electron microscopy-energy dispersive X-ray spectroscopy (SEM-EDS) samples were taken on the Phenom Pro G6 Desktop SEM with acceleration voltage of 15 kV at Advanced Laboratory of Mathematics and Natural Sciences Faculty, Lambung Mangkurat University.

The Brunauer-Emmett-Teller (BET) surface area (S_{BET}) and pore volume (V_p) were measured using N_2 physisorption at -196 °C on a Belsorp Max (BEL Japan). The samples were degassed at 200 °C for 2 h to remove physisorbed gases prior to the measurement. The amount of nitrogen adsorbed onto the samples was used to calculate the S_{BET} via the BET equation. The pore sizes distribution and pore volume was estimated to be the liquid volume of nitrogen at a relative pressure of approximately 0.995 according to Horvath-Kawazoe (HK) approach based on desorption data [25].

The NH_3-TPD was conducted on a Belsorp Max (BEL Japan). The samples were degassed at elevated temperature of 10–200 °C for 2 h to remove physisorbed gases prior to the measurement. The temperature was then kept at 200 °C for 2 h, while flushed with helium gas. NH_3 gas (balanced NH_3, 80% and He, 20%) was introduced at 100 °C for 30 min, then evacuated by helium gas to remove the physisorbed NH_3 also for 30 min. Finally, temperature programmed desorption was conducted at temperature of 100 – 800 °C and the desorbed NH_3 was monitored by TCD.

The H_2-TPR was performed on a Chemisorb 2750, Micromeritics. The samples were heated at 110 °C for 2 h under N_2 stream with flow rate of 40 ml/min, then cooled to room temperature. Before reduction processes, the line was purged

with H_2 (5% Ar gas v/v) for 30 min, then reduced with the same gas (H_2 (5% Ar v/v)) at elevated temperature of 30-700 °C with ramping 10 °C/min. The H_2 uptake was calculated by using calibration curve (H_2 gas; 5% Ar gas v/v, and flow rate of 40 ml/min).

The calculation of the mean metal particle size (d_{VA}) from H_2 can be achieved based on the volume–area mean diameter equation, Eq. (1) [26]:

$$d_{\mathrm{VA}} = \frac{6\upsilon_{\mathrm{m}}}{(Da_m)} \quad (1)$$

where, D is metal dispersion (the ratio of the total number of metal atoms on the support surface to the total number of metal atoms in the bulk sample), υ_m is the volume occupied by a metal atom (m) in the bulk (13.65×10^{-3} nm^3 for Ru)[27] and a_m is the surface area occupied by an exposed surface metal atom (m). The unit cell of hcp Ru has only two atoms and when the (0 0 1) plane is exposed, the surface will have one Ru atom available for H_2 adsorption. When the (1 1 0) plane is exposed, two Ru atoms will be exposed including the atom at the (1/3, 2/3, 1/2) position. In addition, reported results have shown that two other low-index planes, the (0 0 1) and (1 1 0) planes, have similar levels of surface energy compared to the (1 0 0) plane of Ru [20]. Therefore, the (1 0 0), (0 0 1), and (1 1 0) low-index planes may contribute equally to H_2 adsorption. Similar to the treatment by Masthan *et al*. [28] (1 0 0), (0 0 1), and (1 1 0) planes are used to calculate exposed crystal-plane area (am) instead of using only the (1 0 0) plane. Therefore, the surface area occupied by one Ru atom (am) (average from areas of (1 0 0), (0 0 1), and (1 1 0) planes) is 9.09×10^{-2} nm^2 instead of 6.35 x 10^{-2} nm^2 when assuming that only the (0 0 1) plane is exposed.

$$D \text{ (metal dispersion, \%)} = (V_{\mathrm{mon}}/22414) \times S \times M \times 100 / \text{(metal weight\%)} \quad (2)$$

where, V_{mon} = monolayer coverage of H_2 on Ru, cm^3/g STP, M = atomic mass of metal; 101.07 g/mol, and S = stoichiometric factor of H_2 to Ru atom. H_2 is assumed to be dissociatively adsorbed on Ru metal surfaces, which is S = 2, as most researchers use it [28,29].

2.2.3. Catalytic Reactions

Typical catalytic reaction procedure is described as the follows. Catalyst (50 mg), FFalc (2 mmol), dodecane (0.02 mmol), and H_2O (3 mL) as solvent were placed into a glass reaction tube, which fitted inside a stainless-steel reactor. The reactor was flushed with H_2 for ~30 times, after an initial H_2 pressure of 30 bar was introduced at room temperature, the reactor was heated to 180 °C. After 3 h, the reaction mixtures were transferred into sample bin, centrifuged (~5000 rpm for 10 min) and analysed by using GC-FID. The used Ru@TiO_2(R) catalyst was separated using either simple centrifugation or filtration, dried overnight under vacuum at room temperature, and re-activated with H_2 at 400 °C for 2 h prior to reusability testing.

2.2.4. Product Analysis

GC analyses of the reactant (FFalc) and products (1,5-PeD, THFalc, 4,5-DHFM) were performed on a Perkin Elmer Auto System XL equipped with a flame ionization detector and Restek Rtx® BAC Plus 1 capillary column. GC analysis was operated at detector and injector temperatures of 250 °C and 240 °C, respectively, N_2 as a carrier gas (14 mL/min), rates of air and H_2 were 450 ml/min and H_2 45 ml/min, respectively. Products were confirmed by the comparison of their GC and GC-MS retention time and mass spectra with the literatures, except for 4,5-DHFM due to the limitation of commercial availability.

The calibration curve was performed using known concentrations of internal standard (*n*-dodecane), reactant and products to determine the correct response factors. The conversion of FFalc and the yield of the products were calculated according to the following equations:

$$Conversion\ (\%) = \frac{F_0 - F_t}{F_0} \times 100\% \quad (3)$$

$$Yield\ (\%) = \frac{\text{mol of product}}{F_0} \times Conversion\ (\%) \quad (4)$$

where, F_0 is the introduced mol reactant (FFalc), F_t is the remained mol reactant, which are all obtained from GC analysis using an internal standard technique.

3. Results and Discussion

3.1. Screening of Catalyst for Reaction of FFalc to 1,5-PeD

In attempting to find the most suitable heterogeneous supported ruthenium catalyst for aqueous phase hydrogenolysis of furfuryl alcohol to diols (1,2-PeD or 1,5-PeD), we then investigated the effect of various supported Ru catalysts at 180 °C, H_2 30 bar, in H_2O for 3 h. The results of catalytic reaction of FFalc over various supported Ru are summarised in Table 1. At the first experiments, the catalytic reaction of FFalc using a commercially available Ru/C (5 wt% Ru) was conducted and the products were mixture of 2-MeF and 2-MeTHF (46%) and CPO/CPL 21% at 100% conversion of FFalc (entry 1). By using Ru@TiO_2(R) catalyst, 84% of FFalc was converted into 82% CPO/CPL and small amount of side product (others) (2%) (entry 2). Interestingly, a remarkable different of reaction product was

obtained over Ru@TiO_2(A) catalyst under the same reaction conditions. Over this catalyst, the main product was 1,5-PeD (80%) with small amount of 4,5-DHFM (5%) and CPO/CPL (4%) at 87% FFalc conversion (entry 3). The Ru@TiO_2(B) catalyst with structure of brookite, rutile, and anatase phases (TiO_2(B)) for comparison was also synthesised and tested for the reaction of FFalc to 1,5-PeD under the same conditions. An 89% FFalc was converted and the products were distributed to 45% 1,5-PeD, 3% 4,5-DHFM, 15% THFalc, and 26% CPO/CPL (entry 4). Furthermore, ruthenium supported on carbon-doped TiO_2(A) (Ru@C-TiO_2(A)) and carbon-doped TiO_2(R) (Ru@C-TiO_2(R)) catalysts afforded diols (1,5-PeD and 1,2-PeD mixture) and CPO/CPL with total yield of 20-31% and 4-8%, respectively (entries 5-6). These results indicate that the presence of carbon doping affected to the product distribution of FFalc reaction [23].

Catalysts ruthenium-based supported on various metal oxides (*e.g.*, γ–Al_2O_3, ZrO_2, ZnO, and Nb_2O_5) gave THFalc as the main product (65-81%) with 18-22% yield of 1,5-PeD at completed reaction under the same conditions (entries 7-10). Based on these results, it can be presumably concluded that Ru@TiO_2(R) selectively catalysed the furan ring rearrangement to CPO/CPL while Ru@TiO_2(A) promoted the hydrogenolysis of C-O bond of FFalc towards 1,5-PeD or 1,2-PeD. To complete this conclusion, a series investigation on the evaluation of parameter reactions (temperature, initial H_2 pressure, and time profiles) both Ru@TiO_2(R) and Ru@TiO_2(A) catalysts are performed and discussed systematically.

3.2 Evaluation of Reaction Parameters: Ru@TiO_2(R) vs Ru@TiO_2(A)

3.2.1. Effect of reaction temperature

The influence of reaction temperature on the FFalc conversion and product distribution was investigated and the results are shown in Figure

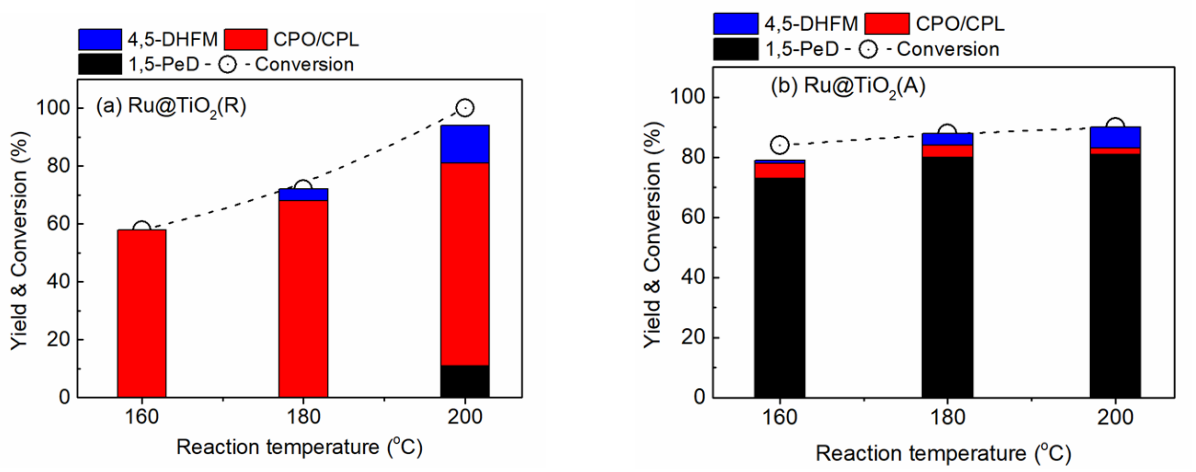

Figure 1. Effect of reaction temperature on the FFalc conversion and yields of 4,5-DHFM, CPO/CPL, and 1,5-PeD over (a) Ru@TiO_2(R) and (b) Ru@TiO_2(A) catalysts. Reaction conditions: Cat. (0.05 g), FFalc (2.0) mmol, H_2O (3 mL), H_2 (30 bar), 160-200 °C, 3 h.

Table 1. Results of selective hydrogenolysis of FFalc using various supported Ru-based catalysts. Reaction conditions: Cat. (0.05 g), FFalc (2.0) mmol, H_2O (3 mL), H_2 (30 bar), 180 °C, 3 h. [a]Conversion and yield were determined by GC (FID) using an internal standard technique. The carbon balance was more than 95% for all the reactions. [b]Others include the condensation product of FFalc (according to the GC-MS data).

Entry	Catalyst	Conv.[a] (%)	Yield[a] (%)					
			1,5-PeD (1,2-PeD)	4,5-DHFM	THFalc	CPO (CPL)	2-MeF (2-MeTHF)	Others[b]
1	Ru@C	100	0	0	0	21	46	33
2	Ru@TiO_2(R)	84	0	0	0	82	0	2
3	Ru@TiO_2(A)	88	80	5	0	4	0	0
4	Ru@TiO_2(B)	89	45	3	15	26	0	0
5	Ru@C-TiO_2(A)	85	26(5)	0	19	18	0	2
6	Ru@C-TiO_2(R)	95	0(20)	0	58	4	5	8
7	Ru@γ–Al_2O_3	100	0(6)	0	71	6	7	4
8	Ru@ZrO_2	100	19	0	81	0	0	0
9	Ru@ZnO	100	22	0	74	0	0	0
10	Ru@Nb_2O_5	100	18	0	65	15	0	2

1. As the Ru@TiO_2(R) catalyst selectively produced CPO/CPL, the influence of reaction temperature was firstly evaluated during FFalc reaction at 160-200 °C, H_2 30 bar for 3 h. The conversion of FFalc smoothly increased as reaction temperature was increased to reach 100% conversion. At 160 °C, the product was only CPO/CPL (58%) at 58% conversion of FFalc. When reaction temperature was increased to 180 °C, the conversion of FFalc slightly increased to 72% to afford 68% CPO/CPL and 4% 4,5-DHFM. However, further increase in reaction temperature to 200 °C caused not only FFalc was increased to 100% but also the formation 1,5-PeD (11%) was also observed while yield of CPO/CPL slightly increased to 70% (Figure 1(a)).

In the case of Ru@TiO_2(A) catalyst, the conversion of FFalc slightly increased as the reaction temperature was elevated from 160 °C to 200 °C to reach 90% FFalc conversion. The yield of 1,5-PeD increased gradually from 73% at 160 °C to 80% and 81% at 180 °C and 200 °C, respectively. Similar to 1,5-PeD yield, the amount of CPO/CPL was nearly constant (4-5%) at the temperature of 160-180 °C, but remaining 2% after reaction temperature was increased to 200 °C. In contrast, yield of 4,5-DHFM increased smoothly as the reaction temperature was increased (Figure 1(b)). These results suggest that catalytic reaction of FFalc using Ru@TiO_2(A) did not depend on the current reaction temperature, which is consistent with the hydrogenation of LA to GVL [30] or hydrogenation of functionalized carboxylic acids [31] using similar Ru/TiO_2 catalyst as reported previously. Therefore, it can be concluded that the optimised reaction temperature for the synthesis of CPO/CPL from FFalc over Ru@TiO_2(R) catalyst was 160-180 °C, while the synthesis of 1,5-PeD from FFalc over Ru@TiO_2(A) catalyst was 180-200 °C. However, further study on the influence of catalyst preparation (e.g., thermal treatment or loading amount) on the catalytic activity and selectivity is important to ensure the role of catalyst structure-activity / selectivity relationship.

3.2.2. Effect of reaction time

The reaction profiles of FFalc conversion as a function of reaction time at 3 h and 5 h over Ru@TiO_2(R) and Ru@TiO_2(A) catalysts are shown in Figure 2. Over Ru@TiO_2(R) catalyst, the conversion of FFalc was 72% to produce 68% CPO/CPL and 4% 4,5-DHFM and 1,5-PeD product was not observed after reaction time of 3 h. After reaction was extended to 5 h, the conversion of FFalc slightly increased to 84% with the main product was CPO/CPL (80%), whereas other products were 1,5-PeD (2%) and 4,5-DHFM (2%) Figure 2(a). The formation small amount of 1.5-PeD and remaining 4,5-DHFM seems likely due to the side reaction of FFalc to 4,5-DHFM then followed by ring opening to 1,5-PeD occurred as the subsequent reaction after 5 h. It has been reported that, the competitive reaction between hydrogenation-hydrogenolysis of furan ring to diols (1,5-PeD or 1,2-PeD) and furan ring rearrangement might be regulated by the surface acidity of catalyst systems, both Brønsted and Lewis acidity [32]. In contrast to Ru@TiO_2(R) catalyst, Ru@TiO_2(A) catalyst exhibited slightly higher FFalc conversion and displayed different product distribution (Figure 2(b)). After 3 h, FFalc conversion was 88% to selectively produce 1,5-PeD (80%), 4% CPO/CPL, and 4% 4,5-DHFM. These results indicate that the reaction of FFalc over Ru@TiO_2(A) catalyst proceeded different pathways.

Nevertheless, the transformation of FFalc may involve two reaction pathways, first, partial

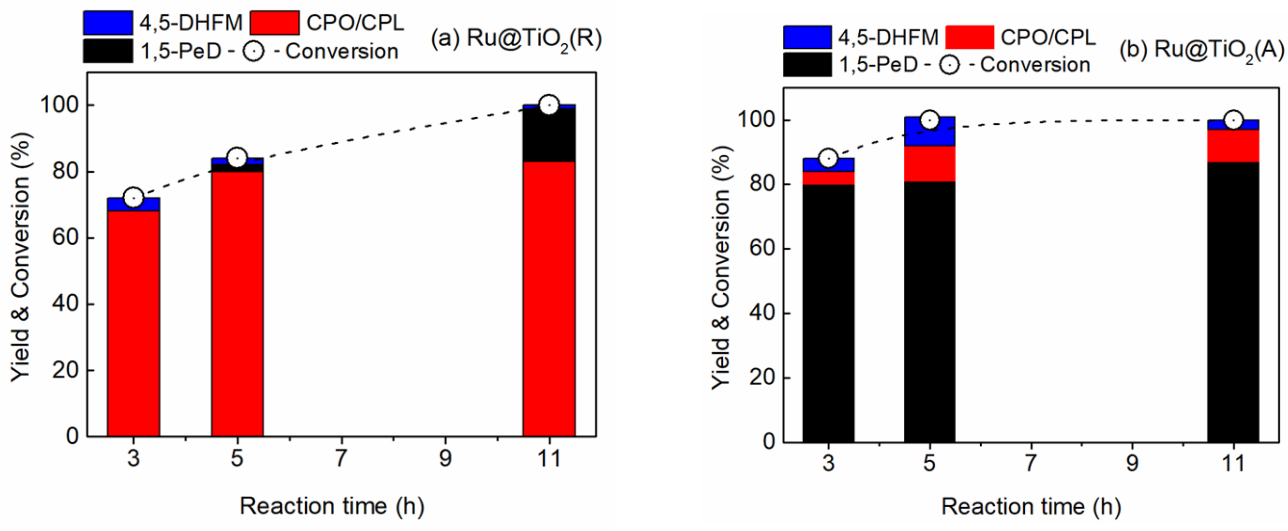

Figure 2. Effect of reaction time on the FFalc conversion and yields of 4,5-DHFM, CPO/CPL, and 1,5-PeD over (a) Ru@TiO_2(R) and (b) Ru@TiO_2(A) catalysts. Reaction conditions: Cat. (0.05 g), FFalc (2.0) mmol, H_2O (3 mL), H2 (30 bar), 180 °C, 3-5 h.

hydrogenation of C=C furan ring to form 4,5-DHFM then followed by the ring opening of C2-O of formed 4,5-DHFM to selectively produce 1,5-PeD [19,33]. Second, furan ring rearrangement on the acidic surface of catalyst to form HCP, then followed by hydrogenation to CPO [34]. To confirm these suggestions, the reaction was extended to 11 h both of catalysts. As expected, Ru@TiO_2(R) catalyst converted 100% FFalc and the products were 16% 1,5-PeD, 83% CPO/CPL, and small amount of remained 4,5-DHFM (1%). On the other hand, Ru@TiO_2(A) afforded 87% 1,5-PeD, 10% CPO/CPL, and 3% 4,5-DHFM at 100% FFalc conversion after 11 h. This indicates that Ru@TiO_2(A) catalyst system preferentially follow the reaction pathways of 1,5-PeD via 4,5-DHFM intermediate which in accordance with the previous work using bimetallic Ru-Sn catalysts [18]. Since the 4,5-DHFM intermediate is not commercially available, the synthesis of 4,5-DHFM using our Ru-Sn catalysts, isolation, purification, and ^{1}H- and ^{13}C-NMR analyses would be the important for the next investigation.

3.2.3. Effect of initial H_2 pressure

The reaction of furan ring of FFalc in the presence of transition metal catalyst strongly affected by hydrogen concentration. At high concentration of H_2 over Ru or Ni-based catalysts proceeded C=C hydrogenation to produce tetrahydrofurfuryl alcohol (THFalc) [19]. The affinity of Ru or Ni-based catalysts towards C=C hydrogenation can be regulated by two simple approaches; modifying with second electropositive metal to form bimetallic alloy [33,35] or constructing on the metal oxide supports that enable strong metal support interaction (SMSI) phenomena [36].

The effect of initial H_2 pressure on the FFalc conversion and yields of 4,5-DHFM, CPO/CPL, and 1,5-PeD over (a) Ru@TiO_2(R) and (b) Ru@TiO_2(A) catalysts is shown in Figure 3. Both Ru@TiO_2(R) and Ru@TiO_2(A) catalysts demonstrated low affinity towards C=C hydrogenation as indicated by the total hindrance of THFalc formation alongside the increase of initial H_2 pressure. By using Ru@TiO_2(R) catalyst, the increase in the initial H_2 pressure to 30 bars resulted the low conversion (72%) but remained high selectivity of CPO/CPL (68% yield). A small amount 4.5-DHFM (4%) was observed without the formation of 1,5-PeD (Figure 3(a)). On the other hand, at lower initial H_2 pressure (10-20 bar), the conversion of FFalc reached maximum. However, while the amount of CPO/CPL remain high (67-75%), the formation of 1,5-PeD significantly increased to 18-25% with 7-8% yield of 4,5-DHFM was remained (Figure 3(a)). Furthermore, similar product profiles were also obtained from hydrogenolysis of FFalc over Ru@TiO_2(A) catalyst. The completed conversion of FFalc (100%) was obtained at initial H_2 pressure of 10 bar with products were distributed to 84% 1,5-PeD, 1% CPO/CPL, and 15% 4,5-DHFM. The amount of 4,5-DHFM increased as the initial H_2 pressure was decreased, whereas CPO/CPL decreased oppositely (Figure 3(b)). These results suggest that the cleavage of C2-O bond of furan ring over both Ru@TiO_2(R) and Ru@TiO_2(A) catalysts preferentially occurred under low concentration of H_2, which consistent with the previous reports [18,20,37]. Therefore, it can be presumably concluded that the optimised reaction parameters for FFalc conversion towards CPO/CPL using Ru@TiO_2(R) was 180 ^{o}C, H_2 30 bar for 3 h, while for the synthesis of 1,5-PeD over Ru@TiO_2(A) was 180 ^{o}C, 10-20 bar H_2 after 3 h.

3.3. Catalyst Structure-Activity Relationship

Figure 4 shows the XRD patterns of Ru@TiO_2(A) (Fig. 4(a)) and Ru@TiO_2(R) (Figure 4(b)) catalysts which were synthesised by using

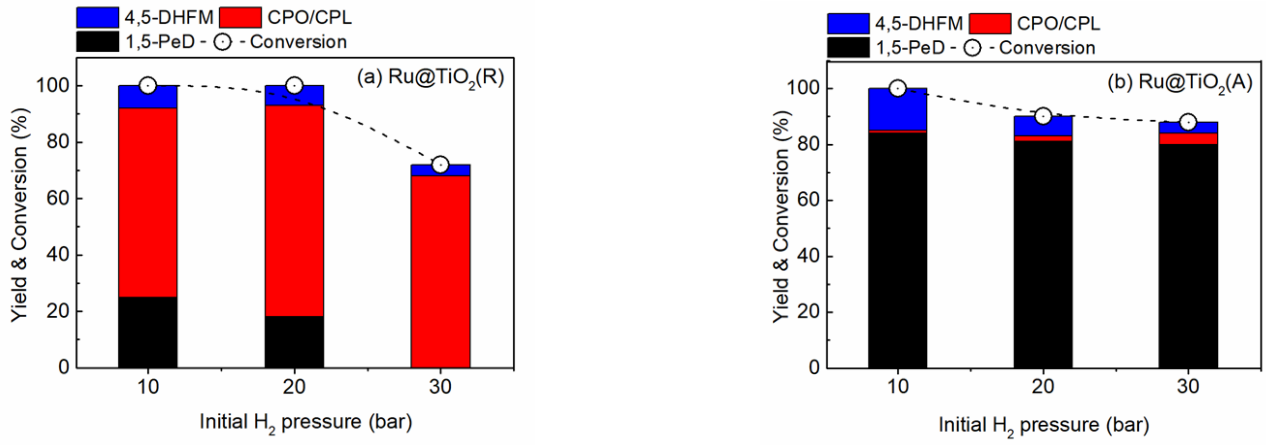

Figure 3. Effect of initial H_2 pressure on the FFalc conversion and yields of 4,5-DHFM, CPO/CPL, and 1,5-PeD over (a) Ru@TiO_2(R) and (b) Ru@TiO_2(A) catalysts. Reaction conditions: Cat. (0.05 g), FFalc (2.0) mmol, H_2O (3 mL), H_2 (10-30 bar), 180 ^{o}C, 3 h.

coprecipitation-hydrothermal from commercially available of TiO_2 rutile (TiO_2(R)) and TiO_2 anatase (TiO_2(A)) at 150 °C for 24 h, followed by reduction with H_2 at 400 °C for 2 h.

The sole structure of anatase in Ru@TiO_2(A) catalyst was clearly observed as indicated by series diffraction peaks of TiO_2(A) phases at 2θ = 25.3°, 37.8°, 48.0°, 54.0°, 55.1°, 62.7°, 68.8°, 70.2°, 75.1°, and 82.8° (JCPDS No. 21-1276) which can be assigned as (101), (112), (200), (105), (211), (204), (116), (220), (215), and (301) planes of TiO_2 anatase phases, respectively (Figure 4(a)). The average crystallite sizes of TiO_2(101) anatase phase at 2θ = 25.3° was 36.2 nm (Table 2). In the case of of rutile as indicated by a series of sharp diffraction peaks at 2θ = 27.32°, 36.06°, 41.28°, 54.36°, 56.40°, 63.10° and 69.38° (JCPDS No. 21-1276) which can be attributed as (110), (101), (111), (211), (220), (002), and (301) planes of TiO_2 rutile phases, respectively (Figure 4(b)). The average crystallite sizes of TiO_2(110) at 2θ = 27.32° in Ru@TiO_2(R) sample was 26.5 nm. A small diffraction peak of metallic Ru(101) was clearly observed at 2θ = 44.06° (JCPDS No. 006-0663) over Ru@TiO_2(R) sample, whereas the diffraction peak of metallic Ru(101) was not observed over Ru@TiO_2(A) sample. This can be attributed to due to strong metal support interaction (SMSI) effect in Ru@TiO_2(A) may dominate than that of in Ru@TiO_2(R), resulting in the coverage of Ru nanoparticles by TiO_x overlayers and leading to higher dispersion RuNPs as it has been previously observed by Lin *et al.* [38] and Azzahra [23].

The hydrogen-temperature programmed reduction (H_2-TPR) of catalysts help to identify the surface species during the hydrogen reduction process. The H_2-uptake, metal dispersion, and particle diameter the synthesised Ru@TiO_2 catalysts are summarised in Table 2. It is found that the specific surface area BET (S_{BET}) derived from N_2 adsorption-desorption for Ru@TiO_2(A) and Ru@TiO_2(R) samples was 37.1 $m^2.g^{-1}$ and 28.2 $m^2.g^{-1}$, respectively (Table 2).

In the case of Ru@TiO_2(A) sample, a high intensity of reduction peak at 73 °C, which can be attributed to the reduction peak of RuO_2 to Ru^0 that interacting with TiO_2(A) support (Figure 5(a)). A broad reduction peak at around 295 °C over this sample was also observed, suggesting typical reduction of RuO_2 with strong interaction with the TiO_2 [39]. The highest reduction peak was observed at 441 °C with low and broad intensity, which can be suggested as the extended-reduction peak of RuO_2 with strong interaction with TiO_2(A). Zhao and co-workers have suggested that the reduction peak at around 400-450 °C due to the strong-metal support interaction (SMSI) phenomena in TiO_2 supported Ru metal catalysts [40]. A series reduction peaks at 276 °C, 323 °C and 441 °C were clearly observed over Ru@TiO_2(R) sample (Figure 5(b)). As similar to the Ru@TiO_2(A) sample, two distinctive reduction peaks at 276 °C and 323 °C were observed, which

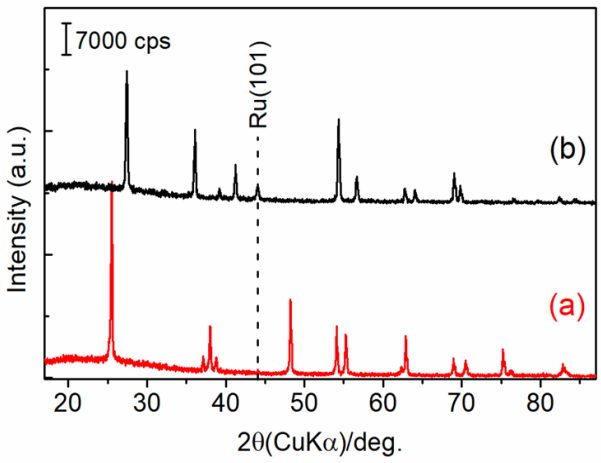

Figure 4. XRD patterns of (a) Ru@TiO_2(A) and (b) Ru@TiO_2(R) catalysts after reduction with H_2 at 400 °C for 2 h.

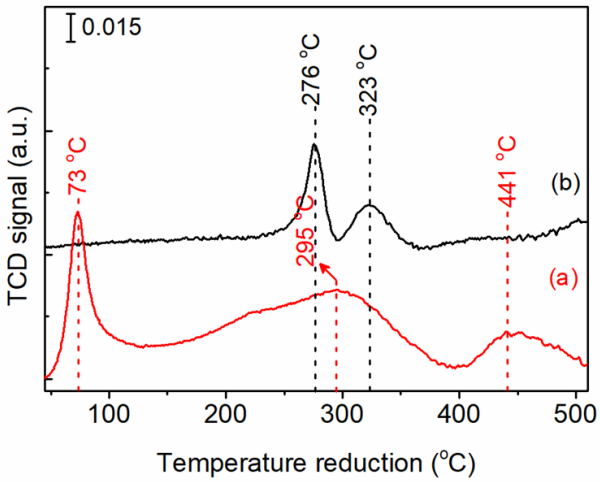

Figure 5. H_2-TPR profiles of (a) Ru@TiO_2(A) and (b) Ru@TiO_2(R) catalysts.

Table 2. Physico-chemical properties (H_2-uptake, metal dispersion, and particle diameter of synthesised Ru@TiO_2 catalysts.

Entry	Catalyst	S_{BET}[a] ($m^2.g^{-1}$)	H_2 uptake[b] ($mmol.g^{-1}$)	D[c] (%)	d_{VA}[d] (nm)	TiO_2[e] (nm)
1	Ru@TiO_2(A)	37.1	1.52	21.4	4.2	36.2
2	Ru@TiO_2(R)	28.2	1.36	11.2	8.3	26.2

[a]Specific surface area BET (S_{BET}), calculated from the amount of adsorbed N_2 from N_2 adsorption-desorption data. [b]The H_2 uptake was derived from H_2-TPR data. [c]Metal dispersion (%). [d]The mean metal particle size (d_{VA}). eAverage crystallite sizes of TiO_2(101) anatase at 2θ = 25.3° and TiO_2(110) rutile at 2θ = 27.3° using the Scherrer`s equation.

can be assigned as the typical reduction of RuO_2 with strong interaction with the TiO_2. However, the reduction peak at 441 °C for Ru@TiO_2(R) is hardly distinguished, suggesting the SMSI phenomena over this sample is less extend and it may less intimate interaction between Ru and TiO_2 surface [41,42]. It is found that the H_2 uptakes of Ru@TiO_2(A) and Ru@TiO_2(R) catalysts were 1.52 mmol.g^{-1} and 1.36 mmol.g^{-1}, respectively (Table 2). The dispersion and particles sizes of Ru metal were also estimated from the H_2 uptake data using the proposed equation of Shen *et al.* with an assumption that the surface area occupied by an exposed surface of Ru(001) [26]. It is found that the dispersion (*D*) of Ru nanoparticles in Ru@TiO_2(A) and Ru@TiO_2(R) was 21.4% and 11.2% with and the mean metal particle size (d_{VA}) of 4.2 nm and 8.3 nm, respectively (Table 2).

The NH_3-TPD profiles were formally divided into three desorption temperature regions to denote three types of acid sites [43,44]: (1) weak acid sites, ranging from 100 to 200 °C, (2) moderate acid sites, ranging from 200 to 350 °C, and (3) strong acid sites, ranging from >350 °C (Figure 6). Both Ru@TiO_2(A) and Ru@TiO_2(R) have similar patterns of desorption peaks with different intensities. A desorption peak at 138-168 °C is assigned as the weak acid sites, and the desorption peak at 214-282 °C is attributed as the strong acid sites. No strong acid sites were observed upon both of samples (Figure 6(b)). The amount of each acid sites and total acid sites are summarised in Table 3. Ru@TiO_2(A) catalyst consisted of 87 µmol NH_3.g^{-1} as the weak acid sites and 112 µmol NH_3.g^{-1} as the medium acid sites (entry 1). On the other hand, Ru@TiO_2(R) comprised 201 µmol NH_3.g^{-1} as the weak acid sites and 707 µmol NH_3.g^{-1} as the medium acid sites (entry 2). The presence large amount of strong acid sites may affect the product selectivity as indicated by the high yield of THFalc and CPO/CPL (Table 1, entry 2). Though the Ru@TiO_2(A) has much lower total acidity of 199 µmol NH_3 per gram than that of Ru@TiO_2(A) (908 µmol NH_3 per gram), whereas the types of acid sites of those catalysts were almost same (Figure 6). Since NH_3-TPD does not allow for the differentiation of Lewis and Brønsted acid sites, pyridine-ATR-IR analysis was conducted on the synthesised catalysts of Ru@TiO_2(A) and Ru@TiO_2(R) and the results are shown in Figure

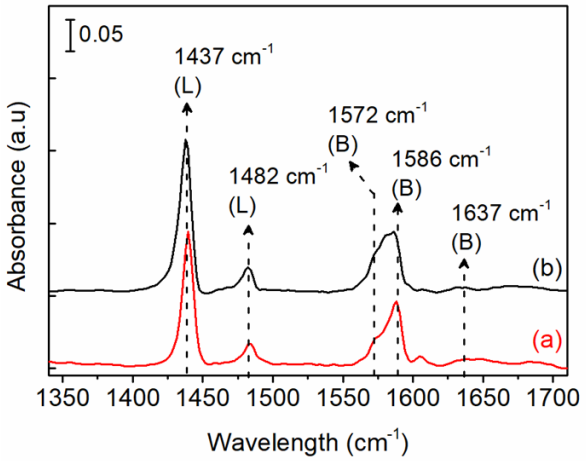

Figure 7. Pyridine-FTIR spectra of (a) Ru@TiO_2(A) and (b) Ru@TiO_2(R) catalysts.

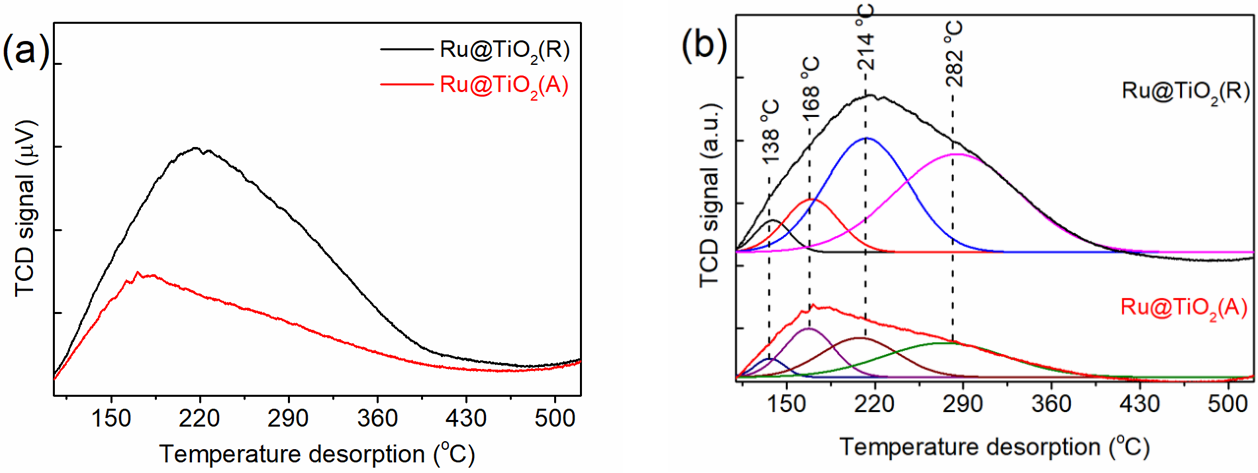

Figure 6. NH_3-TPD profiles of (a) original spectra and (b) deconvoluted spectra of Ru@TiO_2(R) and Ru@TiO_2(A) catalysts, respectively after reduction with H_2 at 400 °C for 2 h.

Table 3. Acidic properties of the synthesised Ru@TiO_2 catalysts. aAcidity was derived from NH_3-TPD spectra according to the formula as reported by Azzouz *et al.* [44].

Entry	Catalyst	Weak[a] (100-200 °C)	Medium[a] (200-350 °C)	Strong (>350 °C)	Total acidity[a] (µmol NH_3.g^{-1})
1	Ru@TiO_2(A)	87	112	-	199
2	Ru@TiO_2(R)	201	707	-	908

7.

According to the literatures on pyridine adsorption peaks in Ru-containing catalysts [45,46] the bands are assigned as follows: the pyridinium ion (PyH^+), which forms from the reaction of pyridine with Brønsted acid sites (B) shows bands around 1647 cm^{-1} (υ_{8a}); coordinatively bound pyridines on Lewis acid sites (L) shows bands around 1445 (υ_{19b}) and 1575 cm^{-1}; and physisorbed or hydrogen-bonded pyridine (H) exhibits bands at near 1437 and 1599 cm^{-1}. The band around 1490 cm^{-1} represents common vibrations from both PyH^+ (B) and coordinatively bound pyridine (L) [47]. The Py-ATR-IR spectrum of Ru@TiO_2(A) confirmed the sole presence of Lewis acid sites, indicated by bands at 1435, 1480, 1586 cm^{-1} [48]. In contrast, the Ru@TiO_2(R) sample displayed the designed bands at 1637 cm^{-1}, signifying the presence of Brønsted acid sites. However, the role distinguished acid site, Brønsted or Lewis acid sites in the catalyst for both Ru@TiO_2(A) and Ru@TiO_2(R) catalysts during FFalc transformation remained unclear. Therefore, the investigations on role of types of acid sites (Brønsted or Lewis) and the detail structure catalyst-activity relationship system are still necessary for future study.

4. Conclusions

We have described the crystal phase-dependence of ruthenium supported on titania (Ru@TiO_2) catalysts on the product selectivity in the aqueous phase hydrogenolysis of furfuryl alcohol was investigated. Two types of TiO_2 with different phases of rutile (R) dan anatase (A) were employed as the support. The Ru@TiO_2 catalysts were synthesised by using coprecipitation-hydrothermal at 150 ^oC for 24 h, followed by reduction with H_2 at 400 ^oC for 2 h. Results of FFalc reaction showed that Ru@TiO_2(R) catalyst produced high yield of CPO/CPL (up to 82%), whereas Ru@TiO_2(R) catalyst afforded 1,5-PeD (80% yield) at 180 ^oC, initial H_2 10-30 bar for 3-5 h. XRD patterns of Ru@TiO_2(A) revealed the sol structure of TiO_2 anatase, while Ru@TiO_2(R) exhibited the presence of Ru(101) and pristine structure of TiO_2 rutile. These suggest that the dispersion of Ru on TiO_2(A) is higher than that of on TiO_2(R), which consistent with results of H_2 uptake, dispersion (D), average diameter of Ru NPs, conversion of FFalc. The presence of higher surface acidity promoted the hydrogenation-rearrangement of furan ring leading to CPO/CPL as the main product as indicated by NH_3-TPD and pyridine-ATR-IR results. This high selectivity of 1,5-PeD over Ru@TiO_2(A) catalyst may be affected by the high dispersion of Ru NPs on TiO_2 facets as depicted by the high H_2-uptake and small particle sizes. Therefore, Further investigations on the role of crystal-phase both of TiO_2(A) and TiO_2(B) using advanced techniques (*e.g.* XPS, FFalc- or CO-DRIFT spectroscopies or HR-TEM) and microkinetic studies are challenging for future research.

Acknowledgment

The authors acknowledge The Indonesian Endowment Funds for Education (LPDP) through BRIN-RIIM2 scheme (contract number of 79/IV/KS/11/2022), DRPTM-Kemendiktisaintek through Regular Fundamental scheme (contract number of 056/E5/PG.02.00.PL/2024), and LPPM-ULM through Internal Fundamental scheme (contract number of 1878/UN8.2/PG/2025) for financial support. We also acknowledge the facilities, scientific and technical support from Advanced Chemical Characterization Laboratory, National Research, and Innovation Agency through E- Layanan Sains - BRIN.

CRedit Author Statement

Author Contributions: Thea Seventina Desiani Bodoi: Writing original draft, Formal Analysis, Investigation, Experiment. Shauqi Aulia Rifwanda, Atina Sabila Azzahra: Formal Analysis, Investigation, Experiment. Rodiansono: Conceptualization, Editing-Review, Supervision. Ferensa Oemry, Gagus Ketut Sunnardianto, Indri Badria Adilina: Advanced Characterisation and Data Interpretation. Takayoshi Hara: Editing-Review, Supervision. All authors have read and agreed to the published version of the manuscript.

References

[1] Gérardy, R., Debecker, D.P., Estager, J., Luis, P., Monbaliu, J.-C.M. (2020). Continuous Flow Upgrading of Selected C2–C6 Platform Chemicals Derived from Biomass. *Chemical Reviews*, 120(15), 7219–7347. DOI: 10.1021/acs.chemrev.9b00846.

[2] Tomishige, K., Nakagawa, Y., Tamura, M. (2017). Selective hydrogenolysis and hydrogenation using metal catalysts directly modified with metal oxide species. *Green Chemistry*, 19(13), 2876–2924. DOI: 10.1039/c7gc00620a.

[3] Xu, C., Paone, E., Rodríguez-Padrón, D., Luque, R., Mauriello, F. (2020). Recent catalytic routes for the preparation and the upgrading of biomass derived furfural and 5-hydroxymethylfurfural. *Chemical Society Reviews*, 49(13), 4273–4306. DOI: 10.1039/d0cs00041h.

[4] Sun, X., Wen, B., Wang, F., Zhang, W., Zhao, K., Liu, X. (2024). Research advances on the catalytic conversion of biomass-derived furfural into pentanediols. *Catalysis Communications*, 187, 106864. DOI: 10.1016/j.catcom.2024.106864.

[5] Tomishige, K., Honda, M., Sugimoto, H., Liu, L., Yabushita, M., Nakagawa, Y. (2024). Recent progress on catalyst development for ring-opening C-O hydrogenolysis of cyclic ethers in the production of biomass-derived chemicals. Carbon Neutrality, 3(17), 1–41. DOI: 10.1007/s43979-024-00090-y.

[6] Zhu, Y., Zhao, W., Zhang, J., An, Z., Ma, X., Zhang, Z., Jiang, Y., Zheng, L., Shu, X., Song, H., Xiang, X., He, J. (2020). Selective Activation of C‐OH, C‐O‐C, or C═C in Furfuryl Alcohol by Engineered Pt Sites Supported on Layered Double Oxides. *ACS Catalysis*, 10(15), 8032–8041. DOI: 10.1021/acscatal.0c01276.

[7] Gilkey, M.J., Mironenko, A.V., Yang, L., Vlachos, D.G., Xu, B. (2016). Insights into the Ring-Opening of Biomass-Derived Furanics over Carbon-Supported Ruthenium. *ChemSusChem*, 9(21), 3113–3121. DOI: 10.1002/cssc.201600681.

[8] He, J., Huang, K., Barnett, K.J., Krishna, S.H., Alonso, D.M., Brentzel, Z.J., Burt, S.P., Walker, T., Banholzer, W.F., Maravelias, C.T., Hermans, I., Dumesic, J.A., Huber, G.W. (2017). New catalytic strategies for α,ω-diols production from lignocellulosic biomass. *Faraday Discussions*, 202, 247–267. DOI: 10.1039/C7FD00036G.

[9] Li, X., Deng, Q. (2023). Review on Metal–Acid Tandem Catalysis for Hydrogenative Rearrangement of Furfurals to C5 Cyclic Compounds. *Transactions of Tianjin University*, 29(5), 347–359. DOI: 10.1007/s12209-023-00367-w.

[10] Xu, W., Wang, H., Liu, X., Ren, J., Wang, Y., Lu, G. (2011). Direct catalytic conversion of furfural to 1,5-pentanediol by hydrogenolysis of the furan ring under mild conditions over Pt/Co2AlO4 catalyst. *Chemical Communications*, 47(13), 3924–3926. DOI: 10.1039/c0cc05775d.

[11] Tong, T., Xia, Q., Liu, X., Wang, Y. (2017). Direct hydrogenolysis of biomass-derived furans over Pt/CeO2 catalyst with high activity and stability. *Catalysis Communications*, 101, 129–133. DOI: 10.1016/j.catcom.2017.08.005.

[12] Tong, T., Liu, X., Guo, Y., Norouzi Banis, M., Hu, Y., Wang, Y. (2018). The critical role of CeO2 crystal-plane in controlling Pt chemical states on the hydrogenolysis of furfuryl alcohol to 1,2-pentanediol. *Journal of Catalysis*, 365, 420–428. DOI: 10.1016/j.jcat.2018.07.023.

[13] Lin, Q., Liu, X.Y., Jiang, Y., Wang, Y., Huang, Y., Zhang, T. (2014). Crystal phase effects on the structure and performance of ruthenium nanoparticles for CO2 hydrogenation. *Catalysis Science and Technology*, 4(7), 2058–2063. DOI: 10.1039/c4cy00030g.

[14] Abdel-Mageed, A.M., Wiese, K., Hauble, A., Bansmann, J., Rabeah, J., Parlinska-Wojtan, M., Brückner, A., Behm, R.J. (2021). Steering the selectivity in CO2 reduction on highly active Ru/TiO2 catalysts: Support particle size effects. *Journal of Catalysis*, 401, 160–173. DOI: 10.1016/j.jcat.2021.07.020.

[15] Cui, B., Wang, H., Han, J., Ge, Q., Zhu, X. (2022). Crystal-phase-depended strong metal-support interactions enhancing hydrodeoxygenation of m-cresol on Ni/TiO2 catalysts. *Journal of Catalysis*, 413, 880–890. DOI: 10.1016/j.jcat.2022.07.039.

[16] Tang, Y., Xu, K., Weng, L., Xu, Y., Tan, L., Wu, L. (2025). Crystal Phase of TiO2 Determines Ni–O–Ti Interface and Enables Nickel Catalysts in Aqueous-Phase Cyclopentanone Synthesis from Furfural. *ChemCatChem*. 17(22), e01205. DOI: 10.1002/cctc.202501205

[17] Amin, B., Aubrecht, J., Kikhtyanin, O., Grechman, E., Alves, G.A.S., Tampieri, A., Föttinger, K., Jędrzejczyk, M., Ruppert, A.M., Ruiz-Zepeda, F., Kubička, D. (2025). Switchable Behavior of Ru–TiO2 Catalysts in HMF Conversion. *ACS Sustainable Chemistry and Engineering*, 13(29), 11652–11667. DOI: 10.1021/acssuschemeng.5c04908.

[18] Rodiansono, R., Azzahra, A.S., Mikrianto, E., Ridhoni, A., Mustari, I., Nurfitriani, A., Bodoi, T.S.D., Sanjaya, R.E., Suarso, E., Ansyah, P.R. (2025). Screening Support of Bimetallic Ruthenium-Tin Catalysts for Aqueous Phase Hydrogenolysis of Furfuryl Alcohol to 1,5-Pentanediol. *Bulletin of Chemical Reaction Engineering & Catalysis*, 20(2), 293–306. DOI: 10.9767/bcrec.20357.

[19] Rodiansono, R., Azzahra, A.S., Santoso, U.T., Mikrianto, E., Suarso, E., Sembiring, K.C., Adilina, I.B., Sunnardianto, G.K., Afandi, A. (2025). Highly efficient and selective aqueous phase hydrogenolysis of furfural to 1,5-pentanediol using bimetallic Ru–SnO x /γ-Al 2 O 3 catalysts. *Catalysis Science & Technology*, 15(3), 808–821. DOI: 10.1039/D4CY01138D.

[20] Bodoi, T.S.D., Azzahra, A.S., Ansyari, M.R., Mikrianto, E., Rodiansono, R., Sanjaya, R.E., Ansyah, P.R. (2024). Selective Conversion of Furfuryl Alcohol to 1,5-Pentanediol Over Ru-Sn/γ-Al2O3-TiO2 : Effect of Calcination Temperature of γ-Al2O3-TiO2. In: *1st ICWDGs2024. AIP Conference Proceedings*, pp. 325–338.

[21] Azzahra, A.S., Dewi, H.P., Mikrianto, E., Sembiring, K.C., Sunnardianto, G.K., Nata, I.F., Rodiansono, R., Jayanudin, J. (2023). Bimetallic Ru-Sn as Effective Catalysts for the Selective Hydrogenation of Biogenic Platform Chemicals at Room Temperature. *Bulletin of Chemical Reaction Engineering & Catalysis*, 18(4), 700–712. DOI: 10.9767/bcrec.20067.

[22] Rodiansono, R., Syahruji, Dewi, H.P., Azzahra, A.S., Sembiring, K.C., Adilina, I.B., Afandi, A. (2024). Pivotal MoOx-decorated Ru/C with a monomeric structure boosts the room temperature and low-pressure hydrogenation of levulinic acid to γ−valerolactone. *Renewable Energy*, 229, 120747. DOI: 10.1016/j.renene.2024.120747.

[23] Azzahra, A.S., Rodiansono, R., Nata, I.F., Sembiring, K.C., Adilina, I.B., Afandi, A. (2025). Thermocatalytic synthesis of 2-butanol from biomass-derived levulinic acid using carbon-doped titania-supported ruthenium. *Sustainable Energy & Fuels*, 9(5), 1279–1292. DOI: 10.1039/D4SE01815J.

[24] Putri, K., Annisa, A., Husain, S., Rodiansono, R. (2020). One-pot Synthesis of Carbon-doped TiO2 with Bimetallic Ni-Ag co-catalysts in Photodegradation of Methylene Blue under UV and Visible Irradiation. *Bulletin of Chemical Reaction Engineering & Catalysis*, 15(1), 35–42. DOI: 10.9767/bcrec.15.1.4811.35-42.

[25] Dombrowski, R.J., Lastoskie, C.M., Hyduke, D.R. (2001). The Horvath–Kawazoe method revisited. *Colloids and Surfaces A: Physicochemical and Engineering Aspects*, 187–188, 23–39. DOI: 10.1016/S0927-7757(01)00618-5.

[26] Shen, X., Garces, L.-J., Ding, Y., Laubernds, K., Zerger, R.P., Aindow, M., Neth, E.J., Suib, S.L. (2008). Behavior of H2 chemisorption on Ru/TiO2 surface and its application in evaluation of Ru particle sizes compared with TEM and XRD analyses. *Applied Catalysis A: General*, 335(2), 187–195. DOI: 10.1016/j.apcata.2007.11.017.

[27] Kellner, C., Bell, A.T. (1982). Effects of dispersion on the activity and selectivity of alumina-supported ruthenium catalysts for carbon monoxide hydrogenation. *Journal of Catalysis*, 75(2), 251–261. DOI: 10.1016/0021-9517(82)90207-X.

[28] Khaja Masthan, S., Rao, R., Chary, V.R., Rao, V., Rao, K. (1994). Influence of metal loading and temperature on hydrogen chemisorption and hydrogenation activity of Ru/gamma-Al2O3 catalysts. *Indian Journal of Chemistry*, 33, 26–32. URL: http://nopr.niscpr.res.in/handle/123456789/40398.

[29] Gueye, I., Kim, J., Kumara, L.S.R., Yang, A., Seo, O., Chen, Y., Song, C., Hiroi, S., Kusada, K., Kobayashi, H., Kitagawa, H., Sakata, O. (2019). Investigation of selective chemisorption of fcc and hcp Ru nanoparticles using X-ray photoelectron spectroscopy analysis. *Journal of Catalysis*, 380, 247–253. DOI: 10.1016/j.jcat.2019.10.004.

[30] Rodiansono, R., Azzahra, A.S., Dewi, H.P., Adilina, I.B., Sembiring, K.C. (2023). MoOx-decorated Ru/TiO2 with a monomeric structure boosts the selective one-pot conversion of levulinic acid to 1,4-pentanediol. *Catalysis Science & Technology*, 13(15), 4466–4476. DOI: 10.1039/D3CY00544E.

[31] Primo, A., Concepción, P., Corma, A. (2011). Synergy between the metal nanoparticles and the support for the hydrogenation of functionalized carboxylic acids to diols on Ru/TiO2. *Chemical Communications*, 47(12), 3613–3615. DOI: 10.1039/c0cc05206j.

[32] Cai, W., Li, Y., Zheng, Q., Song, M., Ma, P., Fang, W., Song, W., Lai, W. (2023). Hydrogenative rearrangement of bioderived furfurals to cyclopentanones over Ni/Nb2O5 catalysts: Promotion effect of reducible NbOx and water. *Fuel*, 338, 127345. DOI: 10.1016/j.fuel.2022.127345.

[33] Rodiansono, R., Azzahra, A.S., Mikrianto, E., Sembiring, K.C., Afandi, A., Sunnardianto, G.K., Adilina, I.B. (2025). One-pot synthesis of confined structure Ru3Sn7 alloys on alumina for exceptionally rapid and selective hydrogenolysis of furfuryl alcohol to 1,5-pentanediol. *Catalysis Science & Technology*, 15(18), 5452–5463. DOI: 10.1039/D5CY00542F.

[34] Astuti, M.D., Kristina, D., Rodiansono, R., Mujiyanti, D.R. (2020). One-pot selective conversion of biomass-derived furfural into cyclopentanone/Cyclopentanol over TiO2 supported bimetallic Ni-M (M = Co, Fe) catalysts. *Bulletin of Chemical Reaction Engineering & Catalysis*, 15(1), 231–241. DOI: 10.9767/bcrec.15.1.6307.231-241.

[35] Rodiansono, R., Dewi Astuti, M., Hara, T., Ichikuni, N., Shimazu, S. (2019). One-pot selective conversion of C5-furan into 1,4-pentanediol over bulk Ni-Sn alloy catalysts in an ethanol/H2O solvent mixture. *Green Chemistry*, 21(9), 2307–2315. DOI: 10.1039/c8gc03938k.

[36] Liu, F., Ftouni, J., Bruijnincx, P.C.A., Weckhuysen, B.M. (2019). Phase-Dependent Stability and Substrate-Induced Deactivation by Strong Metal-Support Interaction of Ru/TiO 2 Catalysts for the Hydrogenation of Levulinic Acid. *ChemCatChem*, 11(8), 2079–2088. DOI: 10.1002/cctc.201802040.

[37] Azzahra, A.S., Annisa, N., Rodiansono, R., Santoso, U.T., Sanjaya, R.E., Suarsa, E. (2024). Effect of Charcoal-Doping on The Yield of 1,5-Pentanediol and Reusability in Ru-Sn/g-Al2O3-Charcoal Catalysts. In: *1st ICWSDGs2024. AIP Conference Proceedings*, pp. 127–138.

[38] Lin, H., Zhang, W., Shen, H., Yu, H., An, Y., Lin, T., Zhong, L. (2024). Control of metal–support interaction for tunable CO hydrogenation performance over Ru/TiO2 nanocatalysts. *Nanoscale*, 16(12), 6151–6162. DOI: 10.1039/D3NR06208B.

[39] Zhan, Y., Zhou, C., Jin, F., Chen, C., Jiang, L. (2020). Ru/TiO2 catalyst for selective hydrogenation of benzene: Effect of surface hydroxyl groups and spillover hydrogen. *Applied Surface Science*, 525 DOI: 10.1016/j.apsusc.2020.146627.

[40] Zhao, S., Ma, H., Qu, W., Tian, Z. (2025). Activity enhancement of Ru/TiO2 catalysts for catalytic hydrogenation of amides to amines through controlling strong metal-support interactions. *Catalysis Science and Technology*, 15(9), 2852–2866. DOI: 10.1039/d5cy00073d.

[41] Luo, Z., Bing, Q., Kong, J., Liu, J.Y., Zhao, C. (2018). Mechanism of supported Ru3Sn7 nanocluster-catalyzed selective hydrogenation of coconut oil to fatty alcohols. *Catalysis Science and Technology*, 8(5), 1322–1332. DOI: 10.1039/c8cy00037a.

[42] Zhou, J., Gao, Z., Xiang, G., Zhai, T., Liu, Z., Zhao, W., Liang, X., Wang, L. (2022). Interfacial compatibility critically controls Ru/TiO2 metal-support interaction modes in CO2 hydrogenation. *Nature Communications*, 13(1) DOI: 10.1038/s41467-021-27910-4.

[43] Watanabe, M., Aizawa, Y., Iida, T., Nishimura, R., Inomata, H. (2005). Catalytic glucose and fructose conversions with TiO2 and ZrO2 in water at 473 K: Relationship between reactivity and acid–base property determined by TPD measurement. *Applied Catalysis A: General*, 295(2), 150–156. DOI: 10.1016/j.apcata.2005.08.007.

[44] Azzouz, A., Nistor, D., Miron, D., Ursu, A. V., Sajin, T., Monette, F., Niquette, P., Hausler, R. (2006). Assessment of acid-base strength distribution of ion-exchanged montmorillonites through NH3 and CO2-TPD measurements. *Thermochimica Acta*, 449(1–2), 27–34. DOI: 10.1016/j.tca.2006.07.019.

[45] Tututi-Ríos, E., González, H., Cabrera-Munguia, D.A., Gutiérrez-Alejandre, A., Rico, J.L. (2022). Acid properties of Sn-SBA-15 and Sn-SBA-15-PrSO3H materials and their role on the esterification of oleic acid. *Catalysis Today*, 394–396, 235–246. DOI: 10.1016/j.cattod.2021.09.008.

[46] Rezayan, A., Wang, K., Nie, R., Lu, T., Wang, J., Zhang, Y., Charles Xu, C. (2022). Synthesis of bifunctional tin-based silica–carbon catalysts, Sn/KIT-1/C, with tunable acid sites for the catalytic transformation of glucose into 5-hydroxymethylfurfural. *Chemical Engineering Journal*, 429, 132261. DOI: 10.1016/j.cej.2021.132261.

[47] Tamura, M., Shimizu, K.I., Satsuma, A. (2012). Comprehensive IR study on acid/base properties of metal oxides. *Applied Catalysis A: General*, 433–434, 135–145. DOI: 10.1016/j.apcata.2012.05.008.

[48] Martin, C., Martin, I., Delmoral, C., Rives, V. (1994). FT-IR Assessment Through Pyridine Adsorption of the Surface Acidity of Alkali-Doped MoO3/TiO2. *Journal of Catalysis*, 146(2), 415–421. DOI: 10.1006/jcat.1994.1079.